Corona based air-flow using parallel discharge electrodes

Van Thanh Dau,[1*] Thien Xuan Dinh,[2] Tung Thanh Bui,[3] Canh-Dung Tran[4], Hoa Thanh Phan[5], and Tibor Terebessy[6]

[1]*Research Group (Environmental Health), Sumitomo Chemical. Ltd, Hyogo, 665-8555, Japan*

[2]*Graduate School of Science and Engineering, Ritsumeikan University, Kyoto, 525–8577, Japan*

[3]*University of Engineering and Technology, Vietnam National University, Hanoi, Vietnam*

[4]*School of Mechanical and Electrical Engineering, University of Southern Queensland, Queensland QLD 4350, Australia*

[5]*Faculty of Electronics Engineering Technology, Hanoi University of Industry, Hanoi, Vietnam*

[6]*Atrium Innovation Ltd., Lupton Road, OX10 9BT, Wallingford, United Kingdom*

E-mail: dauthanhvan@gmail.com

A novel air-flow generator based on the effect of ion wind has been developed by the simultaneous generation of both positive and negative ions using two electrodes of opposite polarity placed in parallel. Unlike the conventional unipolar-generators, this bipolar configuration creates an ion wind, which moves away from both electrodes and yields a very low net charge on the device. The electro-hydrodynamic behaviour of air-flow has been experimentally and numerically studied. The velocity of ion wind reaches values up to 1.25 m/s using low discharge current 5 μA with the kinetic conversion efficiency of 0.65% and the released net charge of -30 fA, 8 orders of magnitude smaller compared with the discharge current. Due to easy scalability and low net charge, the present configuration is beneficial to applications with space constraints and/or where neutralized discharge process is required, such as inertial fluidic units, circulatory flow heat transfer, electrospun polymer nanofiber to overcome the intrinsically instability of the process, or the formation of low charged aerosol.

The principle of ion wind generation using corona discharge was systematically described in 1899 by Chattock with needle-to-plate and needle-to-ring configurations[1]. However, this phenomenon had not achieved active progress until Robinson[2] modelled ion wind generation to calculate the kinetic energy conversion using coupling electro-mechanical parameters. Indeed, many publications reported the characteristics of various electrode arrangements including point-to-plane[3], point-to-grid[4], point-to-ring[5], wire-to-plate[6], wire-to-incline wing[7], where ion wind is generated from a thin wire/needle with high curvature, yielding high velocity of ion wind near the surface of the collector electrode. Many other developments of this method using needle-to-parallel plates[8], point-to-wire[9], rod-to-plate[10], point-to-parallel plate[8], wire-to-cylinder[11], wire-to-wire[12], or point-to-cylinder[13] have been recently suggested. Furthermore, several geometrical improvements of electrodes have also been reported to optimise ion flows by using alternating negative/positive[14], multi electrodes[15].

Ionic winds are most widely used to enhance the heat transfer effect of external flow and a comprehensive review can be seen in the work of Wang et al[16]. In the above systems, one kind of charge particle is dominant and the fundamental requirements is a high-curvature electrode that generates ions and a low-curvature reference electrode placed downstream to define the movement of particles. The discharge ion current and space charge need to be compensated by electrons in the downstream space to eliminate the charging of device[17]. This is sometimes considered as a drawback and a dual positive and negative plasma thruster was proposed to avoid the need for additional neutralization of the system[18], which indeed requires a special electronic power source.

In this paper, a generator of ion wind has been developed using a unique bipolar discharge configuration whose electrodes are symmetrically arranged (Fig. 1). For this configuration, two electrodes of opposite polarity are placed in parallel and generate ions. Hence, both electrodes serve as emitters as well as reference electrodes for generating electric field. This is principally different from multi actuator designs powered from different power sources, providing not only cost savings due to single power source, but also enabling a charge-balanced design with simultaneous charge neutralization in the free space[19]. It is also distinguished from, for example, a

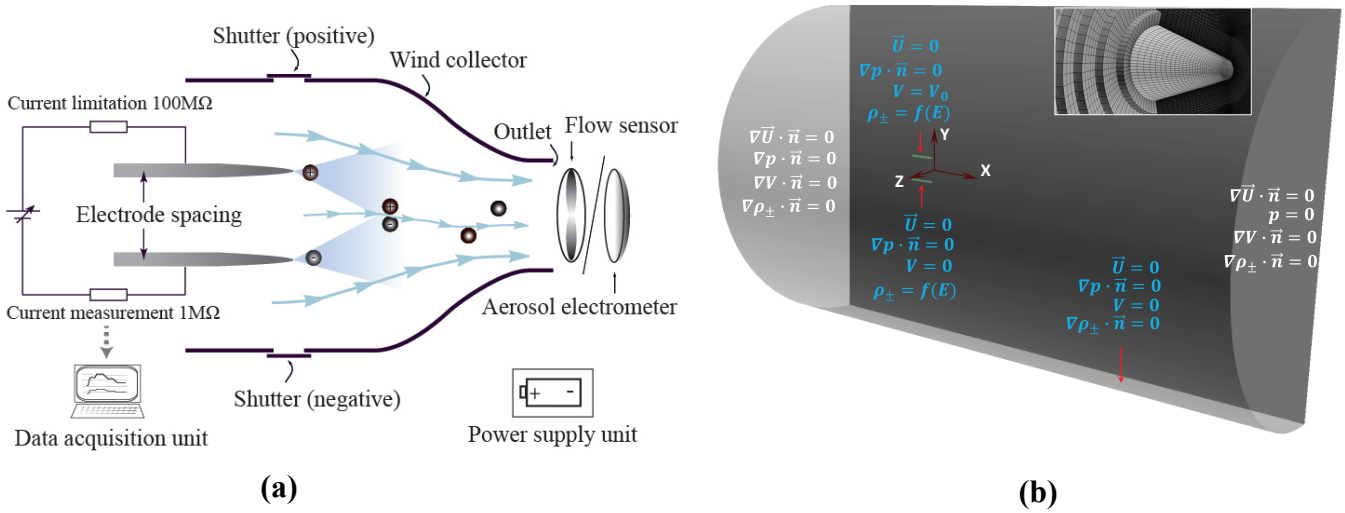

Fig. 1. Bipolar discharge ion wind generator. (a) Experimental setup. (b) Numerical simulation model, a cylindrical domain with diameter and length of ten and twenty times of electrode separation; the inset shows magnified view of mesh at pin tip.

typical needle-to-ring configuration where the neutralization occurred at the reference electrode. The results by our experimental work as well as numerical simulation showed that due to the modified configuration, the ion movement is controlled to be parallel with the axes of the electrodes and away from the device. Because of the high recombination rate of ions[20], the net charge released is very low. Due to easy scalability and low net charge, the present configuration is beneficial to applications with space constraints and/or where neutralized discharge process is required, such as inertial fluidic units[21], circulatory flow heat transfer[22], electrospun polymer nanofiber to overcome the intrinsically instability of the process[23], or the formation of low charged aerosol[24].

The experimental set-up is installed using two identical stainless steel SUS304 pins, each 8 mm long and 0.4 mm in diameter, and placed in parallel as shown in Fig. 1a. Two different kinds of spherical radius (SR) of tips are 15 µm and 80 µm are selected to investigate the effect of pin geometry. The distance between pins is adjustable with a resolution of 0.1 mm using a three axis movable stages TSD-40DC (OptoSigma). A high voltage direct current generator Kopell10 (Kyoshin Denki) is used. A nano-ammeter is also integrated in the voltage generator to measure the discharge current at negative electrode. In order to ensure that the negative charge is accurately measured at the negative polarity and represents the mirror image of positive charge, the entire device is battery operated and insulated from surroundings. The power supply is calibrated using DHM-20 system (Finechem), for a range 0-10 kV.

In order to determine the charge and velocity of the generated ion wind, an aerodynamically shaped collector of 25 mm length, 30×30 mm^2 inlet gate and 15×15 mm^2 outlet gate is used as shown in Fig. 1a. The ion wind is measured by a thermal anemometer ISA-90N (Sibata) installed 10 mm downstream from the outlet gate of the collector. The released charge is alternatively measured at three positions: positive side shutter, negative side shutter and outlet gate, using an aerosol electrometer 3068 (TSI) with sampling rate of 1 Hz. The measurements were performed in steady state discharge condition, verified by monitoring the discharge current throughout the experiment, All the measurements were carried out at 22°C, 55% of relative humidity in atmospheric pressure, the surrounding air is filtered by HEPA filter to minimize background charge and the upstream velocity of the system ambience is always kept under 0.04 m/s. For air movement visualization, smoke is introduced from shutters and the flow is observed by a high-speed camera at a frame rate of 250 fps.

For electro-hydrodynamic simulation, we assume that ion wind is an incompressible turbulent flow of ions and the plasma region, where the gas is ionized in the vicinity of the electrode tips, is modelled by the corresponding charge density. In steady state, the model describing migration of ions within inter-electrode region, their mutual influence on electric field and the charge consumption from recombination process are governed by equations of Gauss' law of electrical field and the conservations of charge, momentum and mass

$$\nabla.\vec{E} = \nabla.\nabla V = -(q_+ - q_-)/\epsilon_0, \quad (1)$$

$$\nabla.\left(\pm\mu q_\pm \vec{E} + q_\pm \vec{U}\right) = \mp R_i q_+ q_- / q_e, \quad (2)$$

$$\nabla\cdot\left(\vec{U}\vec{U}\right) - \nu\nabla.\left(\nabla\vec{U}\right) = (q_+ - q_-)\vec{E}/\rho, \quad (3)$$

$$\nabla.\vec{U} = 0, \quad (4)$$

where ϵ_0 = 8.854×10^{-12} CV^{-1}m^{-1} is the permittivity of free space; μ = 1.6×10^{-4} m^{2}V^{-1}s^{-1} is the mobility of charge; R_i = 10^{-13} m^3 s^{-1} is the rate constant for ion-ion recombination in air; q_e = 1.62×10^{-19} C is the charge of electron; ρ = 1.2041 kgm^{-3} and ν = 15.7×10^{-3} m^{2}s^{-1} are the density and kinematic viscosity of the air, respectively.

It is worth noting that the mutual effects of the electrical field to the ion wind velocity are expressed by $\mu q\vec{E}$ and $q\vec{U}$ where q, $\vec{E}$, $\vec{U}$ are the charge density, electric field strength and the ion wind velocity, respectively. Neglecting any external bulk flow and the ion diffusion, the charge drift creates an electric current density $\vec{J} = \overrightarrow{J_+} + \overrightarrow{J_-}$, satisfying the continuity condition $\nabla.\vec{J} = 0$. Eqs (1)-(4) were discretised in 3-dimensional space using the far field boundary condition as shown in Fig. 1b. The voltage is applied on the boundary of the electrodes. The charge density condition is computed from the experimentally measured current $q_{\pm} = \mathrm{I}/(\mu E_{\mathrm{on}} A)$, A is the total area on the electrode where the electric field is greater than corona onset determined by Peek's law for air E_{on} = 3.23×10^6 Vm^{-1}. For the velocity of ion wind, the wall condition is non-slip at the electrodes and zero pressure is at the others. The numerical simulation of the problem was carried out using an in-house code developed from OpenFOAM library.

Figure 2a presents two typical relationships between the voltage and current ($I/V \propto V$ (the Townsend relation) and $\sqrt{I} \propto V$) using the present configuration with electrode spacing of 6 mm and pin tips SR = 15 μm. As can be seen, while the relationship $I/V \propto V$ is non-linear (concave upward), a linear behavior was observed for $\sqrt{I} \propto V$ over the whole measured range of the voltage except at very low current.

The relationship $I/V \propto V$ was used in the analysis of various configurations including point-to-plane [2], point-to-grid[25], point-to-ring[26]. Although the relationship $\sqrt{I} \propto V$ has not frequently appeared in recent publications, it was used to assess the ion wind generation in several configurations, for example the positive corona with electrode distance 50 mm by Kip[27] and the negative corona with electrode distance less than 15 mm by Ferreira[3] for the configuration point-to-plane. Thus, the relationship $\sqrt{I} \propto V$ is used to analyze the present configuration in the next sections.

The simulation of the ion wind by the present configuration is illustrated in Fig. 2b together with a glowing corona image at the negative pin tip in laboratory (iv). After generated at the vicinity of tips, ion clouds (charged particles) gain an initial momentum to move in the direction away from the pin tips (i) & (i') and in parallel with the electrodes. Indeed, the glowing discharge as shown in Fig. 2b (iv) reveals that pin tips are similar to spheres embedded on pins and the right hemisphere of tip with extremely high curvature focuses the electric field outwards and nearly parallel to the pin axis. Under the impact of the electric field, the clouds of oppositely charged ions from two electrodes (ii) & (ii') tend to impinge on each other in between electrode interspace (iii). Here, the charge is mostly consumed by ion recombination and the bulk flow of ions moves forward. The flow is visualized by the motion of smoke particles input via side shutters. A recorded video, available as a supplementary material, confirmed that the air movement is in good agreement with the simulated result.

The generated charge measured from shutters was very high, more than ±12500 fA respectively for positive and negative side, exceeding the maximum range of aerosol electrometer and showing that both charges are generated simultaneously (Fig. 2c). As a result of the mixing of opposite charges, the total charge of the ion wind after the outlet of the wind collector was very low. It was typically around -30 fA and was very small compared with the discharge current (on the order of μA). This confirms that the positive and negative charges were well balanced.

Figure 2d depicts the relationship between the velocity of ion wind and the discharge current. In this work, we focused on the use of low currents below 10 μA where the ionization only occurs at the close vicinity pin tips. Experimental results in Fig. 2d showed that the velocity of the ion wind U increases linearly with the square root of current $\sqrt{I}$ for currents less than 5 μA but nonlinearly for higher currents. Furthermore, the numerical simulation was in good agreement with experimental results for low currents. At higher currents, the ionized region around the negative pin expands and the streamer around positive pin propagates outwards and towards counter electrodes [28]. This leads to a significant decrease of the kinetic conversion efficiency of ion wind along

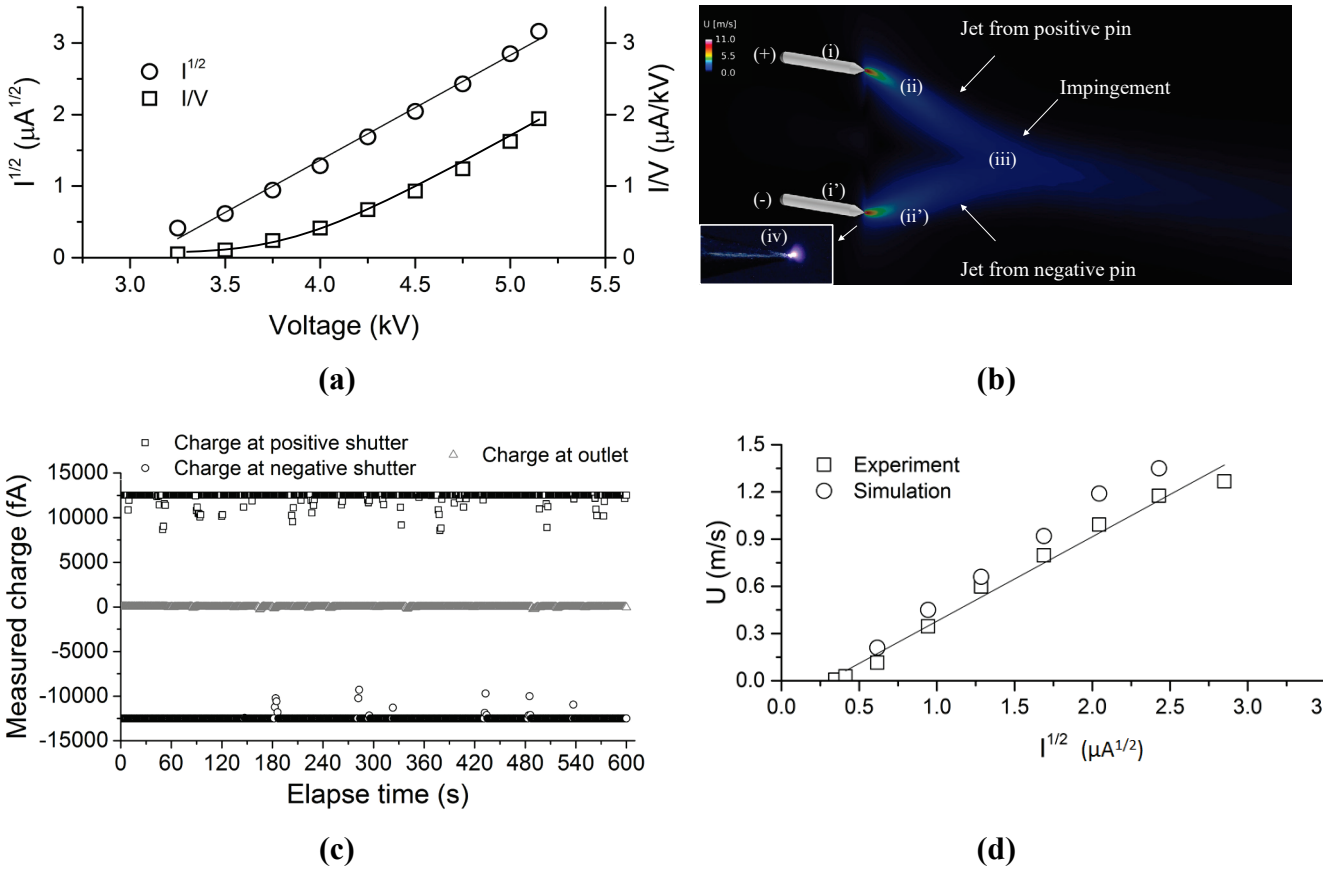

Fig. 2. Result for pin tip SR = 15 μm. (a) Voltage – current for electrode separation of 6 mm. (b) Velocity field simulation of the ion wind generation with parameters given in Fig. 2a. (i) & (i') pin tips; (ii) & (ii') jet of ion clouds; (iii) impingement point and (iv) glowing corona image taken at negative pin tip with applied voltage of 4.5 kV and discharge current of 4.0 μA. (c) Charge measurement results. (d) The ion wind velocity plotted versus $\sqrt{I}$.

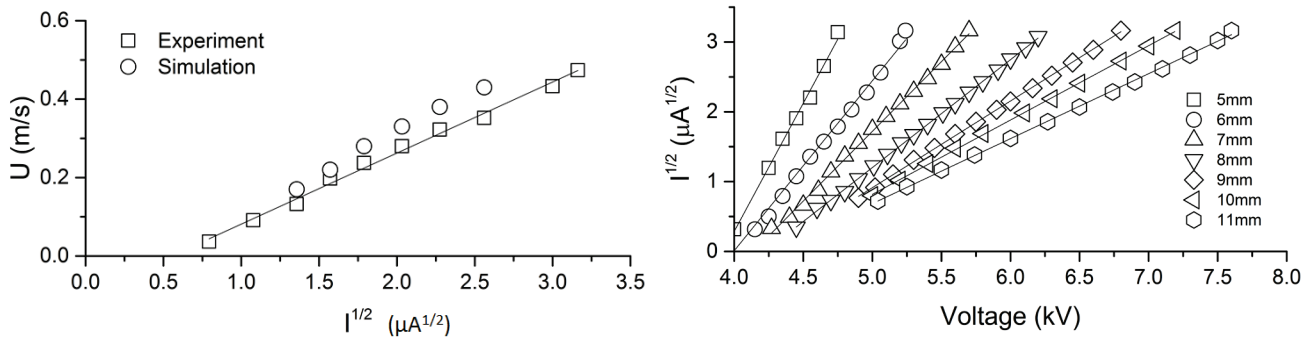

(a) **(b)**

Fig. 3. Results for pin tip SR = 80 μm. (a) The ion wind velocity plotted with $\sqrt{I}$ for electrode separation of 6 mm. (b) The $\sqrt{I}$ plotted with the discharge voltage V for a range of electrode separation from 5 to 11 mm.

the direction parallel with the pin axis.

The same experimental work and numerical simulation has been carried out using pin tip SR of 80 μm (Fig. 3a). The lower velocity of ion wind confirmed the previous conclusions. Because of bigger tip radius, the electric field between pins increases the velocity of charged particles in the electric field direction and then decreases the kinetic conversion efficiency in the direction parallel with pin axis. Furthermore, Fig. 3a confirmed a linear relationship between the velocity of ion wind and $\sqrt{I}$ as stated in the previous experiment. These results are in good agreement with the work by Robinson[2] using the analytical formula $U = \mathrm{k}\sqrt{I/\rho\mu}$, where k is a constant depending on electrode configuration.

The influence of several geometrical parameters of pins on the relationship $\sqrt{I} \propto V$was also considered in Fig. 3b, which plots $\sqrt{I}$ versus V using pins of 80 μm rounded tips over a range of 5-11 mm pin separation. Results in Fig. 3b showed that (i) the relationship $\sqrt{I} \propto V$ is linear with any electrode separation and (ii) the gradient of $\sqrt{I} - V$ increases with the diminution of electrode separation. From the latter statement, it may be concluded that by reducing electrode separation, lower voltages can be applied to reach a desired current value and consequently a desired ion wind velocity. This yields a scaling-down for the dimension of device.

In order to investigate the efficiency of the system using the present configuration, the relationship between the corona discharge power and the velocity of the ion wind was analyzed. The efficiency of the system is defined as the kinetic energy conversion ratio and given by

$$\eta = \frac{\mathrm{P_o}}{\mathrm{P}_i}, \qquad (5)$$

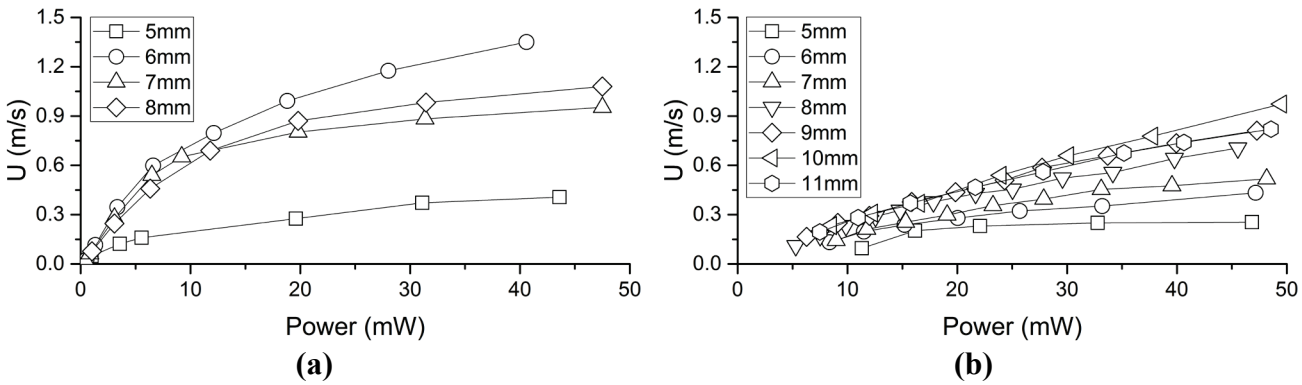

Fig. 4. Velocity of ion wind U plotted with the applied power with (a) pin tip SR = 15 μm and a range of electrode separations from 5 to 8 mm; and (b) pin tip SR = 80 μm and a range of electrode separations from 5 to 11 mm.

where $P_o = \frac{1}{2}\rho \int_{A_0} U^3 dS$ is the output mechanical power of ion wind; *S* is the cross-section of outlet; $P_i = V \times I$ is the input corona discharge power.

Figure 4a presents the velocity of ion wind with respect to the applied power using pin tip SR of 15 μm with a range of electrode separations from 5 mm to 8 mm. While the generated ion wind tends to strengthen with the decrement of electrode separation as stated above, the results described in Fig. 4a indicate an optimal distance 6 mm in terms of power efficiency. Fig. 4b shows the experimental data obtained from the same set-up using rounded pins with SR of 80 μm. The results showed that the optimal electrode separation for this case is 10 mm. Since the ionized region with larger pin tip diverges, the velocity of ion wind and the efficiency of system reduce in comparison with those described in Fig. 4a. This finding is in good agreement with the above discussions.

Experimental results showed that by using two sharp pins with 6 mm electrode separation, a discharge current of 5 μA was able to generate ion wind with velocity up to 1.25 m/s. Hence, the corresponding efficiency is about 0.65% compared with 0.4%, 1.72% and 0.015% for point-to-ring[5], point-to-grid[4], and wire-to-converging plate[7], respectively.

It is worth noting that as a result of the mixing of opposite charges (Figs. 2b-2c), the total charge of ion wind after the outlet for the bipolar configuration is almost independent on the electrode separation in experiments. It is only around 10 times of the value of the background, which was measured after turning off the device in the filtered ambient environment

In conclusion, a corona based air-flow generator using symmetrically arranged electrodes has been developed and evaluated. The air-flow generator is based on the simultaneous generation of both positive and negative ions using two sharp electrodes placed in parallel. Advantages of the configuration include: (i) reduction of the power consumption; (ii) generation of neutralized ion wind and (iii) applicable for neutralized discharge process such as corona discharge, electrospray or electrospinning. To the best of our knowledge, this kind of discharge configuration using symmetrically arranged electrodes is uniquely reported for the first time in this research area.

References

[1] A.P. Chattock, Philos. Mag. Ser. 5 **48**, 401 (1899).

[2] M. Robinson, Trans. Am. Inst. Electr. Eng. Part I Commun. Electron. **80**, 143 (1961).

[3] G.F.L. Ferreira, O.N. Oliveira, and J. a. Giacometti, J. Appl. Phys. **59**, 3045 (1986).

[4] E. Moreau and G. Touchard, J. Electrostat. **66**, 39 (2008).

[5] H. Kawamoto and S. Umezu, J. Electrostat. **66**, 445 (2008).

[6] D.B. Go, S. V Garimella, T.S. Fisher, and R.K. Mongia, J. Appl. Phys. **102**, (2007).

[7] C. Kim, K.C. Noh, J. Hyun, S.G. Lee, J. Hwang, and H. Hong, Appl. Phys. Lett. **100**, (2012).

[8] D.H. Shin, J.S. Yoon, and H.S. Ko, Int. J. Heat Mass Transf. **84**, 35 (2015).

[9] I.Y. Chen, M.Z. Guo, K.S. Yang, and C.C. Wang, Int. J. Heat Mass Transf. **57**, 285 (2013).

[10] H. Toyota, S. Zama, Y. Akamine, S. Matsuoka, and K. Hidaka, IEEE Trans. Dielectr. Electr. Insul. **9**, 891 (2002).

[11] B. Kim, S. Lee, Y.S. Lee, and K.H. Kang, J. Electrostat. **70**, 438 (2012).

[12] J. Darabi and C. Rhodes, Sensors Actuators, A Phys. **127**, 94 (2006).

[13] L. Li, S.J. Lee, W. Kim, and D. Kim, J. Electrostat. **73**, 125 (2015).

[14] C. Kim, K.C. Noh, S.Y. Kim, and J. Hwang, Appl. Phys. Lett. **99**, 2013 (2011).

[15] D.F. Colas, A. Ferret, D.Z. Pai, D. a. Lacoste, and C.O. Laux, J. Appl. Phys. **108**, 0 (2010).

[16] H.C. Wang, N.E. Jewell-Larsen, and A. V Mamishev, Appl. Therm. Eng. **51**, 190 (2013).

[17] K. Nishiyama and H. Kuninaka, Trans. Japan Soc. Aeronaut. Sp. Sci. Aerosp. Technol. Japan **10**, Tb_1 (2012).

[18] D. Rafalskyi and A. Aanesland, Appl. Phys. Lett. **106**, 104101 (2015).

[19] V.T. Dau and T. Terebessy, US20140151471A1 (n.d.).

[20] B.M. Smirnov and H.S.W.M. Sir., *Negative Ions* (1982).

[21] V.T. Dau, D.V. Dao, T. Shiozawa, and S. Sugiyama, IEEE Sens. J. **8**, 1530 (2008).

[22] V.T. Dau, T.X. Dinh, and T.T. Bui, Sensors Actuators B Chem. **223**, 820 (2015).

[23] O. Salata, Curr. Nanosci. **1**, 25 (2005).

[24] V.N. Morozov, J. Aerosol Sci. **42**, 341 (2011).

[25] K. Yamada, J. Appl. Phys. **96**, 2472 (2004).

[26] P. Giubbilini, J. Appl. Phys. **64**, 3730 (1988).

[27] A.F. Kip, Phys. Rev. **55**, 549 (1939).

[28] R.S. Sigmond, J. Appl. Phys. **56**, 1355 (1984).